An Experimental Apparatus for Bench-Scale Fire Testing Using Electrical Heating Pads

Aleksandra Seweryn (ORCID) *, Department of Urban and Environmental Engineering, Liège University, Quartier Polytech 1, All. de la Découverte 9, 4000 Liège, Belgium*

Andrea Lucherini, Department of Structural Engineering and Building Materials, Ghent University, 9000 Ghent, Belgium and Department for Research of Fire-Safe Sustainable Built Environment (FRISSBE), Slovenian National Building and Civil Engineering Institute (ZAG), 1000 Ljubljana, Slovenia

Jean-Marc Franssen, Department of Urban and Environmental Engineering, Liège University, Quartier Polytech 1, All. de la Découverte 9, 4000 Liège, Belgium

Abstract. This research study concerns an experimental, budget-friendly, electricity-powered apparatus for bench-scale fire testing. The apparatus consists of various elements, of which the most important are ceramic heating pads, used to impose heat fluxes on exposed surfaces of specimens. The test method allows to control the heating pads' temperature and to adjust the distance between the heating pads and the specimen to obtain well-defined heat fluxes up to 50–60 kW/m^2. Higher heat fluxes and temperatures can be obtained by setting the heating pads in *full power mode*, with or without the use of a thermal shield, which can lead to heat fluxes up to 150 kW/m^2. The heating and thermal boundary conditions imposed by the apparatus are characterised and discussed, and the thickness of the convective boundary layer at the heating pads' surface is estimated significantly lower than in the case of gas-fired radiant panels. The performance of the apparatus is analysed for various conditions: controlling the temperature of the heating pads, in an open environment or with the presence of thermal shields, and in *full power mode*. A few examples of application of the apparatus to fire test typical construction materials (steel and glass) are also presented. These results emphasise the well-defined heating conditions in temperature-controlled mode. The study finally discusses the advantages and limitations of the apparatus, as well as many possibilities of future applications and improvement for future research studies.

---

* Correspondence should be addressed to: Aleksandra Seweryn, E-mail: aleksandra.seweryn@doct.uliege.be

1. Introduction

Fire safety is an important field of construction engineering which aims at reducing the risk of death, health injuries and property damages due to fire. An important part of fire safety focuses on understanding how construction materials can contribute to fire growth and spread (reaction to fire) and how construction elements perform when exposed to a flashover fire (fire resistance) [1]. Many researchers are continuously investigating the performance at high temperatures and/or under fire conditions of various, sometimes very complex, materials. This problem is usually solved through material testing at various scales.

As regards fire resistance tests, the standard practice foresees expensive and time-consuming full-scale standard furnace fire tests [2]. However, before opting for the standard procedure, it is common to carry out several fire tests at bench-scale because of their lower temporal and economic cost. This approach is usually at the core of research and development projects for new and innovative materials.

Bench-scale fire testing typically implies the application of heat fluxes, either constant or following specified time histories, to replicate various heating conditions and fire exposures. It is important to control the applied heat flux during fire testing to accurately analyse and compare the behaviour of various materials at elevated temperatures. In fire science, the easiest way to do it is to control and apply a radiative heat flux at an exposed surface of test specimens, and this can be achieved in two ways. First, keeping the same geometry, the temperature of the radiative body can be changed, therefore the radiative heat flux changes as well following the Stefan–Boltzmann law. Otherwise, the temperature of the radiative body can be kept to a specific level and the desired heat flux evolution is obtained through the variation of the view factor between the specimen and the heating surface, for instance by changing the relative distance between the two [3].

There are many test methods which follow this principle and the most common include the cone calorimeter and the Fire Propagation Apparatus (FPA). The cone calorimeter, which uses a conical metallic electrical resistance, is limited to impose constant incident heat fluxes because of its high response time due to the high thermal inertia of the electrical resistance [4]. The heat flux is imposed on specimens of $10\,10$ cm^2 by controlling the temperature of the conical metallic electrical resistance. Many researchers have tested a vast range of materials, imposing heat fluxed up to 100 kW/m^2 [5]. Another piece of equipment to study the flammability of materials and products is the Fire Propagation Apparatus (FPA) [6, 7]. The size of specimens tested is the same, $10\,10$ cm^2, but, unlike the cone calorimeter, the heat flux is supplied using infrared heating lamps. In this case, the radiative heat flux at the specimen surface is controlled by the power provided to the heating lamps.

Furthermore, there are other types of equipment for fire testing that use various types of radiant panels of various sizes to investigate the flammability of construction materials. Examples are the test method for the determination of the burning behaviour of flooring [8, 9] and the Lateral Ignition and Flame Spread Test (LIFT) apparatus to study the lateral flame spread on building products [10–12].

Another method was proposed at the beginning of the century by Sakji [13, 14], further developed and extensively used at the University of Edinburgh [15] where it was given the name of Heat-Transfer Rate Inducing System (H-TRIS). The H-TRIS test method is an apparatus that uses gas-fired radiant panels to impose well-defined thermal boundary conditions, usually constant or varying time histories of incident heat flux. This is possible by changing the distance between the radiant panel and the specimen surface, therefore the view factor. The specimen is often tested in a vertical configuration, convenient for materials which are typically used in this configuration, such as glass panels and windows [16]. Apart from the ability to impose a wide range of heating regimes, H-TRIS offers many other advantages compared to traditional large-scale testing: reduced financial and temporal costs, high experimental repeatability, and ease of visual inspection (open environment). Thanks to its important advantages, H-TRIS has been widely adopted around the world in research and development studies which included, among others, analysis of concrete spalling, intumescent coatings, thermal insulation materials, timber structures and glass structures [17–25].

Nevertheless, there are some limitations connected with the widespread use of H-TRIS. Firstly, its relatively-high cost makes it usually inaccessible for research teams with little financial availability. Moreover, occupational health and safety concerns are raised due to the presence of gas burners, often not allowed in laboratories that are not specifically built for fire testing, for example, laboratories shared by several departments. Finally, even when testing non-combustible materials, there is often the need for an exhaust hood to remove the combustion gases coming from the gas-fired panels. These shortcomings make H-TRIS in some cases an unsuitable solution and leave researchers with limited testing capabilities.

For these reasons, a similar apparatus to H-TRIS but powered by electricity has been designed, easy to maintain, budget-friendly, and at the same time able to provide repeatable and reliable experimental results. This study presents the characteristics of this apparatus, including a technical description of the assembly and the testing method. The advantages, as well as the shortcomings, over other well-established fire testing methods are highlighted and discussed. In conclusion, this research study also presents a few examples of fire testing applications and discusses ideas for future developments.

2. Materials and Methods

2.1. Apparatus Description

The experimental apparatus designed and assembled in the Fire Laboratory of Liège University (Belgium) is shown in Fig. 1. It underwent a set of improvements in order to optimise its performance before its involvement in research projects.

As shown in Figs. 1 and 2, the apparatus consists of:

1. A 70 55 cm^2 vertical steel plate on which two layers of 5 ceramic heating pads strips (Mannings, CP24, 61 8.5 cm^2 each) are fixed. The steel plate is attached with bolts to two steel profiles (each 100 cm long) which have a support func-
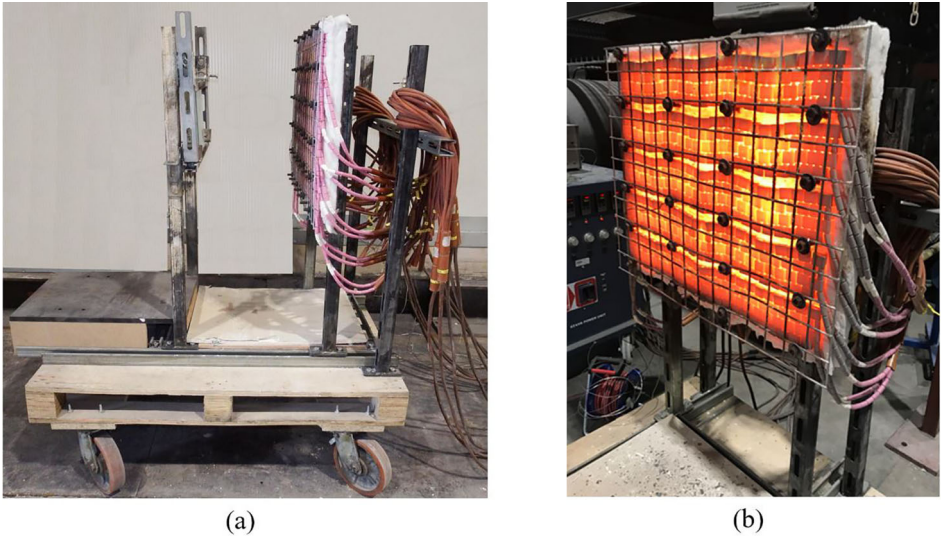
(a)   (b)

Figure 1. Photography of the experimental apparatus (a) side view, (b) front view of the heating surface.

tion. Two layers of ceramic fibre insulation (Insulfrax S Blanket—25 mm thick) are placed between the heating pads and the steel plate. A steel grid is mounted with bolts to keep the heating pad strips at a specific location. The resulting heating surface is $61\,46$ cm^2.

2. A steel frame serving as a specimen holder, assembled with steel profiles of various shapes and lengths, the longest being 100 cm. It allows to keep the specimens in a vertical position, parallel to the heating surface and at a specific distance.

3. A Mannings 65 kVA transformer unit is used to power and control the temperature in the heating pads. The temperature of the heating pads can be controlled in six different zones independently. When 10 heating pads are used, only five different zones are controlled: two heating pads (same location over the heating surface but different layers) are connected to each zone of the transformer. All zones had the same settings.

4. A wooden base on wheels is used to support and easily move the described apparatus.

Two sets of different heating pads were considered. The first ones, *standard Mannings CP24 heating pads*, were made of nickel-chrome alloy, allowing a nominal maximum temperature of 1050°C according to the producer. This limitation in temperature, plus the fact that they are fragile and tend to break after a few utilizations close to the maximum allowed temperature, were the reasons to opt for the *high-temperature Mannings CP24 heating pads* with the heating wire made of Kanthal alloy. These heating pads have a nominal maximum temperature of 1300° C, can provide faster heating rates, and are more robust with limited failure.
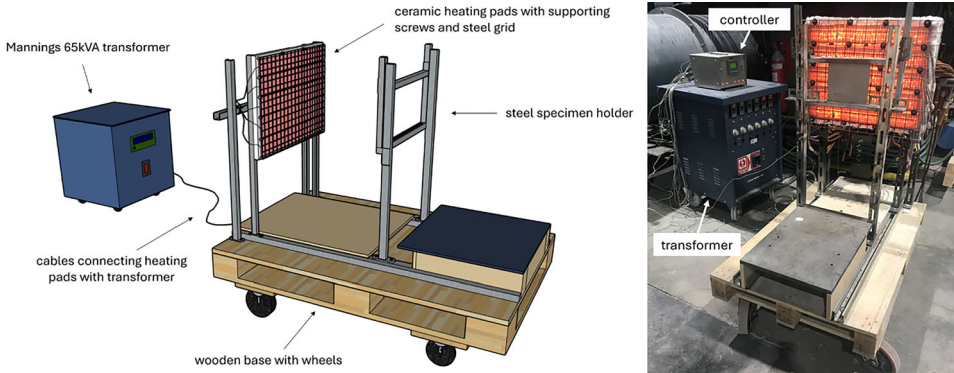
Figure 2. Schematic illustration (left) and photography (right) of the experimental apparatus and its components.

Their higher price (60 € vs. 25 € per heating pad at the time of writing) is easily compensated by the higher durability.

Heating pads can be mounted as one layer or two layers, as shown in Fig. 3, or even more. To achieve temperature and heat fluxes comparable to the ones usually applied in fire testing (e.g. H-TRIS or cone calorimeter which use heat fluxes in the range of 50–100 kW/m^2[5, 15]), it was found that at least two layers of heating pads were necessary. In this case, the inner layer reaches higher temperatures than the outer layer due to the lower heat losses at the heating pads' surface. For example, when the temperature of the exposed surface of the outer layer is about 800°C, the inner layer typically reaches temperatures of about 1000°C. With the available power and current size of the heating surface, the maximum number of heating pad layers is four. With full power mode in an open environment, for the distance of 10 cm between the heating pads and the heat flux gauge, the maximum incident heat flux obtained for one layer is around 27 kW/m^2, for two layers around 57 kW/m^2 and for three layers around 67 kW/m^2. However, having more than two layers is associated with a bigger risk of heating pad failure due to overheating in the inner layer. In order to reduce the maintenance time and the risk of pad failure during experimental tests, the decision was taken to limit the number of layers to two for the current apparatus.

2.2. Control Parameters

To determine specific heating regimes for fire testing, three parameters can be controlled: the temperature of the heating pads, the distance between the heating pads and the specimen, and the use of different specimens and specimen holders.

2.2.1. Temperature of the Heating Pads The first parameter which can be controlled in order to apply specific heating conditions on the exposed surface of the specimen is the temperature of the heating pads. The measurement and control of
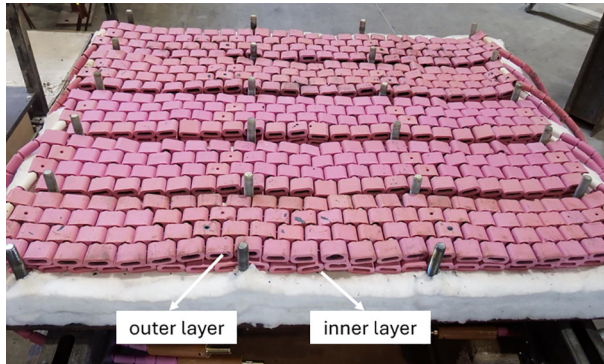
Figure 3. Positioning of two heating pads layers: outer layer and inner layer.

the temperature of the heating pads is not a trivial process and various methodologies were attempted to provide representative and repeatable measurements.

The heating pads are manufactured with special holes in the ceramic beads (see Fig. 4). These holes are primarily used for the placement of thermocouples which measure and control the temperature of the heating pads. However, it was discovered that this method did not provide robust temperature measurements because, in identical experimental conditions, temperature variations up to about 200°C were observed depending on little changes in the position of the thermocouple inside the hole of the heating pad.

Thus, various methods of thermocouple attachment (shielded type-K thermocouples, nominal diameter 1.5 mm) in the heating pads were studied to find the most thorough way to measure and control the temperature of the heating pads, easy to reproduce from test to test and from the calibration to test.

a. The first method of thermocouple placement includes attaching five thermocouples in the dedicated holes, very close to the surface of the heating pads (Fig. 4a).

b. The second method foresees attaching the thermocouples on the surface of the heating pads with insulation pads placed between the steel grid and the ceramic elements to ensure contact between the thermocouple and the heating pads' surface (Fig. 4b).

c. The third method consists of attaching the thermocouples between the ceramic beads of the heating pads and touching the second layer of the heating pads (Fig. 4c).

d. In the last method, thermocouples are placed in the dedicated holes, far from the surface of the heating pads aiming at measuring the temperature between the two layers of the heating pads (Fig. 4d).

Figure 5 presents a comparison of temperatures recorded according to different methods of thermocouple attachment in the heating pads with a set temperature
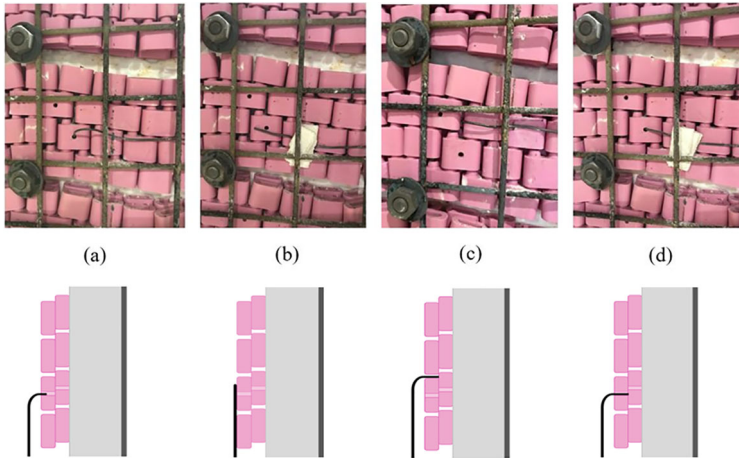
Figure 4. Four different methods of thermocouple attachment in the heating pads.

equal to 950°C using method (d) and in steady-state conditions (after 24 min from the start of the heating process, explained in Sect. 3). Method (a) has proven to be the least reproducible due to the large measured temperature range (from about 760°C up to 940°C). On the other hand, method (b) causes fluctuations of about ± 30°C, while methods (c) and (d) have shown a similar range of temperature, with more fluctuations in method (c) because of slight thermocouple movements. Finally, method (d) was chosen to measure the representative temperature. This method aims at measuring the temperature of the solid elements in the heating pads. This avoids the influence of convection effects due to the hot gas flows and secures the thermocouple at a specific location, avoiding movements. In this way, fluctuations of the reading and inaccuracies were limited. The temperature range to be obtained with this method can be directly associated with the local temperature differences in the heating pads (± 20°C).

The selected thermocouple attachment method was implemented for all five zones of the heating pads, as shown in Fig. 6. The temperature in each zone was recorded and/or controlled separately with a thermocouple of the same type.

Once defined the method to measure and control the temperature of the heating pads, the apparatus offers two different ways to impose various heating regimes: manually and automatically.

1. The *manual mode* does not control the temperature of the heating pads during the transient conditions, and it only aims at a defined target temperature. To achieve the target temperature, it applies the highest heating rate which can be delivered by the transformer (approx. 50°C/min). This mode is limited by the
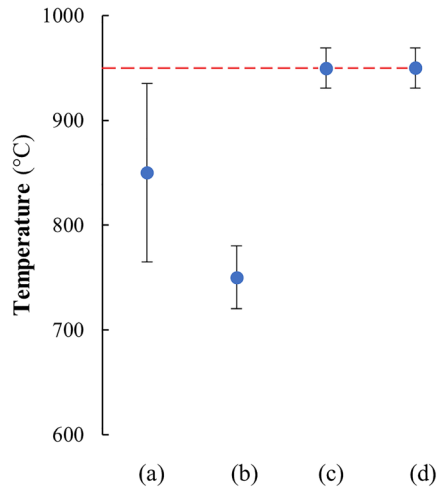
Figure 5. Comparison of temperatures recorded with a set temperature equal to 950˚C, in steady-state conditions, with different methods of thermocouple attachment in the heating pads.
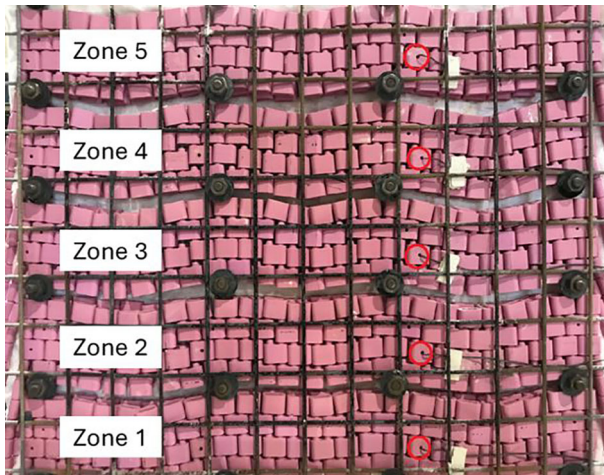

Figure 6. Five thermocouples inserted in holes in order to measure and/or control the temperature of the heating pads in five zones.

maximum target temperature that can be set. In this setup and using the described transformer, it is possible to set the target temperature of the heating pads up to 950°C due to the technical limitation of the transformer. When this target temperature has been reached, the transformer supplies the heating pads with the amount of power needed to maintain the specified temperature in steady-state conditions. The manual mode can be also used without defining any target temperature, referred to in the following sections as *"full power mode"*, even though only about half of the power of the transformer is used with the current number and size of the heating pads.

2. The *automatic mode* uses a controller connected to the transformer (see Fig. 2). The controller allows to impose a pre-defined temporal evolution of the temperature of the heating pads, following a linear evolution (constant heating rate). In this case, the minimum and maximum nominal heating rates that can be applied to the heating pads are 1°C/h and 1000°C/h respectively. The specified target temperature can then be maintained at a given constant level in a precise way.

The heating rate and target temperature are controlled separately for five utilised zones, and it has been observed that, with the dimensions of the radiant panel and the specimens described within this research study, a rather uniform heating on the specimen's surface is obtained when all zones are set to follow the same evolution. For example, Fig. 7 shows the temperature distribution on the surface of the heating pads captured using an infrared camera (Optris PI 400i), placed at a distance approximately 60 cm from the heating pads and setting a unit emissivity. It emphasises the temperature uniformity over the whole surface of the heating pads, excluding the areas within 3 cm from the edges and the securing steel bolts (between 660 and 880°C measured locally over this surface).

2.2.2. Distance Between Heating Pads and Specimen Similarly to H-TRIS, the distance between the heating pads and the specimen is the second parameter crucial to determine the level of heat flux reaching the exposed surface of the test specimen [15]. The change in distance between the heating pads and the exposed surface of the test specimen affects the view factor between these two surfaces [3]. Hence, the radiation component that is emitted by the heating pads' surface and reaches the exposed surface of the test specimen is lower for higher distances. The further the specimen is placed from the heating pads, the lower the view factor, therefore lower incident heat flux at the exposed surface of the test specimen.

As the heat flux intensity, also the distribution of heat flux over a surface is affected by the change in relative distance between the heating pads' surface and the target test surface. For closer distances, the heat flux intensities are higher, but its distribution is less homogeneous, also being affected by discontinuities on the radiating surface (e.g., hot and cold spots). For further distances, the heat flux distribution is typically more homogeneous because the heating pads' surface tends to behave as a point source of radiation.

In the present configuration shown in Fig. 2, the distance between the heating pads and the specimen holder can only be modified before and/or after each test.
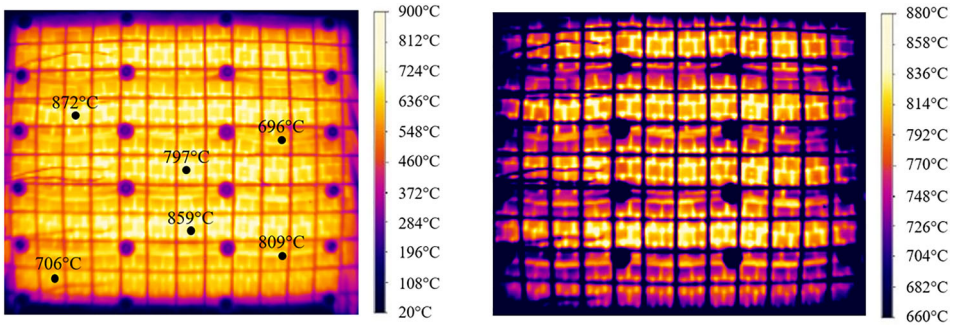
Figure 7. Temperature distribution on the surface of the heating pads, captured by the infrared camera.

Within this study, the distance was varied between 6 and 50 cm. Limited modifications of the support system of the specimen holder would also allow to vary the distance also during a test, for example with the implementation of a step motor which can directly control the stand-off distance between the exposed surface of the test specimen and the heating pads' surface with fast response and high accuracy, similarly to H-TRIS [15].

2.2.3. Thermal Feedback It is important to mention that, when the temperature of the heating pads is not controlled and the heating pads are fed with a specific electrical power from the transformer (like in the case of *full power mode*), the system tends to a specific temperature that is controlled by the net heat gain at the heating pads. In turn, the energy balance at the heating pads directly depends on various factors, hence the heat losses and gains at the heating pads. Since the heat gains are fixed (specific electrical power), the temperature evolution of the heating pads is controlled by the heat losses. This is the case if various objects are placed in front of the heating pads, and they provide radiation feedback and/or convective heat transfer. Accordingly, the temperature of the heating pads (and consequently the heating conditions) can be affected by the presence of a specimen, the type of specimen, the size of the specimen, the presence of a thermal shield (e.g., insulating fibre mats around the specimen), and the distance between the specimen and heating pads [26]. This means that the temperature evolution on the heating pads is not directly regulated, and the thermal boundary conditions may vary from test to test (with the same provided electrical power). In particular, the influence of the specimen and the thermal shield in front of the heating surface can be related to different modes of heat transfer. A specimen or a thermal shield can provide radiation feedback to the heating pads by heating up at the exposed surface and affecting the radiative heat transfer. In contrast, the boundary layer of the specimen and the thermal shield can interact with the thermal boundary layer of the heating pads and tested specimen, affecting the convective heat transfer. In

turn, the problem is also affected by the distance between the heating pads and the specimen. All these effects are experimentally investigated in Sects. 3.3 and 3.4.

2.3. Calibration Process

In order to quantify the thermal boundary conditions produced by the heating pads in different conditions, a heat flux gauge (Hukseflux SBG01) was used to calibrate the apparatus. The water-cooled heat flux gauge was placed in the steel specimen holder in front of the centre of the heating surface to estimate the incident heat flux. The heat flux gauge itself was calibrated in the range of 20–100 kW/m^2. Outside this range, the heat flux gauge produced results with lower accuracy. As an example, the heat flux measurement at room temperature shows a value of around 5 kW/m^2 and should be disregarded.

3. Thermal Exposure Quantification and Definition

To calibrate the assembled apparatus, various measurements of incident heat flux were performed in order to estimate the thermal conditions produced by the heating pads in different configurations. First, the temperature or the provided electrical power was controlled at the heating pads in an "open environment". This condition refers to the situation in which there was no specimen or thermal shield placed in front of the heating pads, just the water-cooled heat flux gauge for calibration (supported by the specimen holder). Afterwards, various specimens and thermal shields were added in front of the heating pads to understand their influence.

3.1. Temperature Control and Open Environment

First, the heating pads were studied in an "open environment" and the temperature of the heating pads was controlled to different target values to investigate the influence of the heating mode. Two cases were compared. The automatic mode was set with a nominal heating rate of 1000°C/h and a target temperature of 800°C, while the manual mode was set with a target temperature of 950°C. In both cases, the temperature evolution of the heating pads was recorded and controlled in all five zones, and the heat flux gauge was placed in front of the heating surface, at a distance of 10 cm. The results of both measurements are shown in Fig. 8. The reported error bars for the temperature measurements include the thermocouple accuracy specified by the producer ($\pm$ 4°C up to 1000°C), fluctuation of thermocouple readings, and differences in temperature distribution between the five heating pad zones. A similar approach is followed for all the other thermocouple measurements reported within this study.

Figure 8 shows that the time needed to reach the temperature stabilisation at 950°C with manual mode was about 24 min, whereas the target temperature of 800°C was achieved after about 46 min when the automatic mode was applied (constant heating rate of about 17°C/min). It is possible to calculate manually the stabilization time for the automatic mode (constant heating rate), while for the
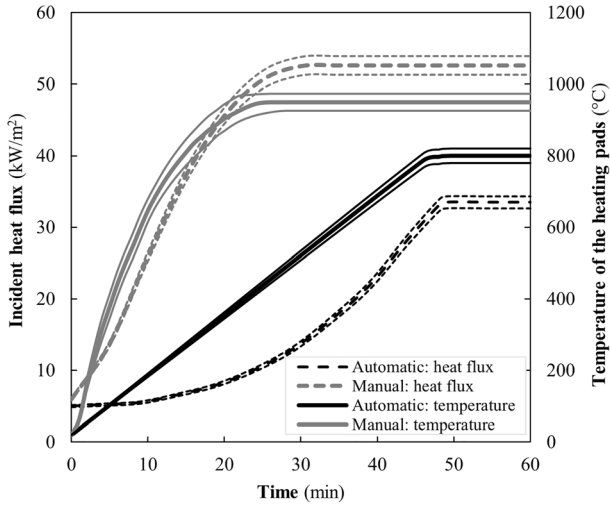
Figure 8. Temperature of the heating pads and incident heat flux measured at 10 cm distance for two different heating modes: automatic (heating rate 1000°C/h and stabilised temperature 800°C) and manual (target temperature 950°C).

manual mode, the heating rate is not controlled, and the stabilisation time depends on the specific target temperature.

During these measurements, it was observed that the temperatures in all five zones followed different evolutions depending on the mode. The manual mode does not control the heating rate, therefore the temperature alignment in the different heated zones is carried out by the transformer once the target temperature is achieved. On the other hand, in the automatic mode, the temperatures in the different heated zones are always aligned and follow analogous evolutions, from the beginning of the heating and following the same heating rate. This results in higher inaccuracies of the temperature evolution measurement for manual mode compared to automatic mode, as shown in Fig. 8.

In order to measure the incident heat flux as a function of the distance between the heating pads and the heat flux gauge, the transformer was set to the manual mode with various target steady-state temperatures: 800°C, 850°C, 900°C and 950°C. The stabilisation time for each of the target temperatures was different, in the range between 15 min (800°C) and 24 min (950°C). The results of the incident heat flux measurements for the above-mentioned target temperatures as well as for *full power mode* (explained in Sect. 3.2) are shown in Fig. 9. The reported error bars for the heat flux measurements include fluctuations in the heat flux reading and the heat flux calibration accuracy (± 1.5 kW/m^2).

For each of the target temperatures, there is a clear parabolic relationship visible between the incident heat flux and the distance between the heating pads and the heat flux gauge. Figure 9 also highlights how, in temperature-controlled mode, the heating pads can apply incident heat fluxes up to about 50 kW/m^2 (at a 10 cm
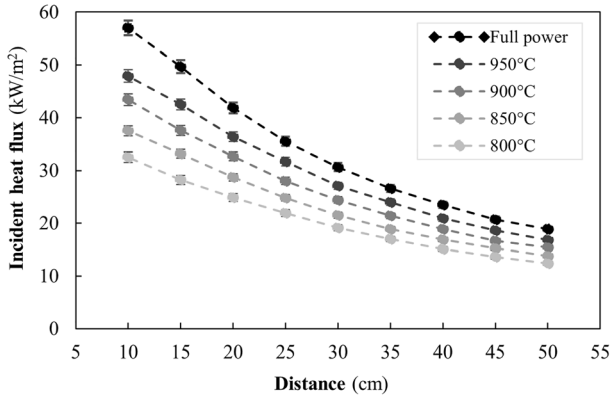
Figure 9. Incident heat flux measured for various distances in an open environment, steady-state condition, for controlled temperature on the heating pads of 800°C, 850°C, 900°C and 950°C as well as full power mode.

distance). As expected, this value decreases if the distance to the heating pads is increased or the heating pads' temperature is reduced.

The apparatus calibration was performed for distances from 10 to 50 cm to target the heat flux range in which the heat flux gauge was calibrated (20–100 kW/m²). An attempt was made to calibrate it for distances below 10 cm. However, in this case, the heat flux gauge was placed too close to the heating pads and it was almost certainly affected by the interaction with the thermal boundary layer of the heating pads (discussed in Sect. 4.1.2). Additionally, at such a small distance, the discontinuities on the heating pads' surface can have a more important influence on the results of the heat flux calibration (values and distributions).

The relationship between the incident heat flux and the temperature of the heating pads, for distances from 10 to 50 cm between the heating pads and the heat flux gauge, was also estimated and shown in Fig. 10. As expected, the highest heat flux is reached for the smallest distance (10 cm) and the highest temperature (950° C). The closer the distance, the higher the difference in the incident heat flux due to the change in target temperature.

3.2. Full Power Mode and Open Environment

A similar process to measure the incident heat flux as a function of the distance between the heating pads and the heat flux gauge was carried out with the heating system set on *full power mode*.

First, the transient evolution of the temperature of the heating pads was recorded and the heat flux was measured at three different distances between the heating pads and the heat flux gauge: 10, 20 and 30 cm. Figure 11 shows how the heating pads tended to approximately 1000°C. In this case, the stabilisation time for achieving steady-state condition was about 45 min and this is visible in all the heat flux curves at different distances. The highest heat flux achieved for the *full*
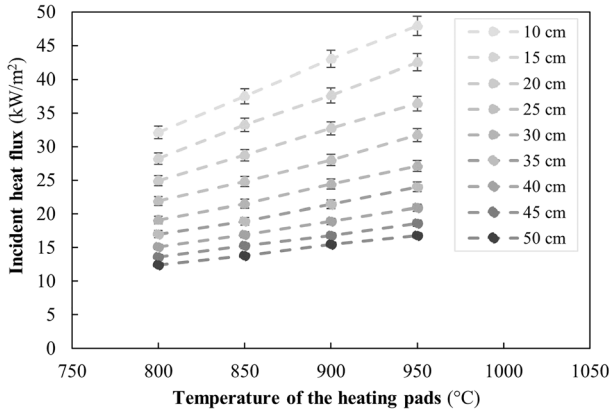
Figure 10. Incident heat flux measured in an open environment, steady-state condition, for controlled temperature on the heating pads of 800°C, 850°C, 900°C and 950°C and various distances.
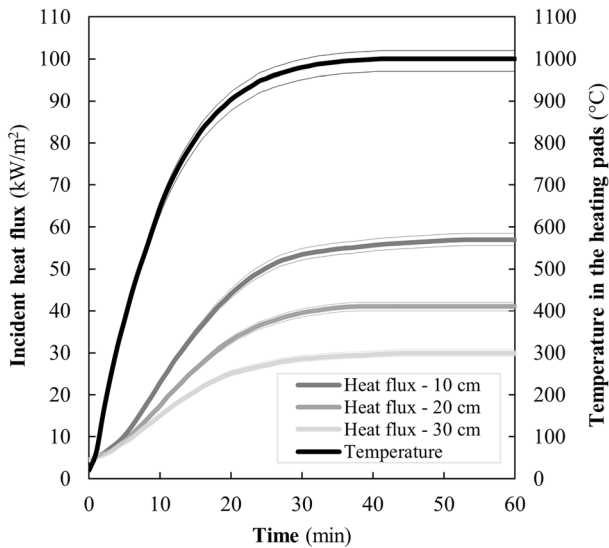

Figure 11. Evolution of temperature in the heating pads and the incident heat flux for distances 10 cm, 20 cm and 30 cm between the heat flux gauge and the heating pads.

power mode at the closest distance (10 cm) was about 57 kW/m^2, significantly higher than for the distance 20 cm (about 41 kW/m^2) and 30 cm (about 30 kW/ m^2). This plot underlines how the *full power mode* allowed higher temperatures at the heating pads, leading to higher heat fluxes that can be achieved in the same experimental conditions. As in the temperature-controlled mode, a similar curve can be also added to the calibration curves shown in Fig. 9, again highlighting the

higher temperatures and heat fluxes that the heating pads' surface can produce in *full power mode*.

3.3. Full Power Mode and Specimen

As mentioned in Sect. 2.2.3, when the heating pads are set in *full power mode* and their temperature is not directly controlled, the temperature evolution of the heating pads is affected by the environment around the heating surface. For example, this is the case if the specimen holder and a specimen are placed in front of the heating pads. In addition, considering a fixed specimen holder of limited surface area, this phenomenon is primarily affected by the specimen type and size, as well as the distance between the heating pads and the specimen's exposed surface.

In order to investigate this problem, the temperature in the heating pads was monitored when testing 20 20 cm^2 planar specimens (i.e. plates) placed in front of the thermocouple in zone 3. Different materials were tested to study the influence of the material thermo-physical properties on the temperature of the heating pads. Four different plates were tested: stainless steel plate (thickness 2 mm), carbon steel plate (thickness 5 mm), glass plate (thickness 6 mm) and ceramic fibre plate (thickness 25 mm).

As reported in Table 1, the tested materials cover a wide range of material surface optical properties (i.e. emissivity/absorptivity) and thermo-physical properties (e.g. thermal inertia). Indeed, in conditions where radiative heat transfer is dominant, these variables are key for the temperature evolution at the exposed surface of tested specimens [3].

It should also be stressed that in the steel and ceramic fibre cases, the tested materials can be considered opaque and gray bodies, hence their transmissivity is null and their emissivity can be assumed as their absorptivity value (Kirchhoff's law) [3]. However, it is not the case for glass. Depending on the wavelength of the radiation electromagnetic waves, a part of the radiation is absorbed, a part is reflected, and a part is transmitted through its thickness. For near-infrared and infrared wavelengths, it has been shown how the glass transmission typically decreases for elevated temperatures, compared to room temperature, and as a result, the absorption increases [27].

First, the local change in temperature of the heating pads' surface during testing can be visually detected from the difference in colours on the heating pads' surface (see Fig. 12).

Then the difference in temperature of the heating pads with and without any interaction with the exposed specimen is analysed. The initial temperature measurement was carried out at the distance of 50 cm between the heating pads and the specimen, and the stabilisation time to reach steady-state conditions was set to 45 min. Afterwards, the specimen was moved closer to the heating surface, with 5 cm steps, and the temperature measurement was performed for 5 min after reaching steady-state conditions at each distance. It was noticed that the specimen holder alone also affected the temperature evolution, so it was also tested without any material specimen.

Table 1
Material Surface Optical and Thermo-Physical Properties of Tested Materials (Ambient Temperature)

Material	Carbon steel [28]	Stainless steel [28]	Glass	Ceramic fibre
Emissivity (−)	0.7	0.4	0.84 [29]	0.4–0.6 [32]
Reflectivity (−)	0.3	0.6	0.16	0.4–0.6
Transmissivity (−)	–	–	0.23 [34]	–
Absorptivity (−)	0.7	0.4	0.61	0.4–0.6
Density (kg/m^3)	7850	7850	2500 [29]	128 [30]
Specific heat (J/kg K)	440	455	720 [29]	1000 [31]
Thermal conductivity (W/m K)	53.33	14.85	1 [33]	0.05 [30]
Thermal inertia (J/m^2 K s$^{1/2}$)	13,570	7290	1342	80

Figure 12.   Test on stainless steel specimen: temperature difference visible on the surface of the heating pads through difference in the colour of the ceramic elements.

The two plots of Fig. 13 report the temperature increment in the heating pads for all the investigated cases, compared to the values in the open environment (only water-cooled heat flux gauge in front of the heating surface). The results underline how the specimen holder alone caused an increase in the temperature of the heating pads measured in zone 3 by about 20°C for the distance of 10 cm between the specimen holder and the heating pads, and for distances above 25 cm, no temperature increment was observed. In contrast, for the glass and ceramic fibre specimens, the temperature change was already visible at a distance of 30 cm, whereas the cases of carbon steel and stainless steel were comparable to the specimen holder one. Nevertheless, temperature increments above 70°C at a
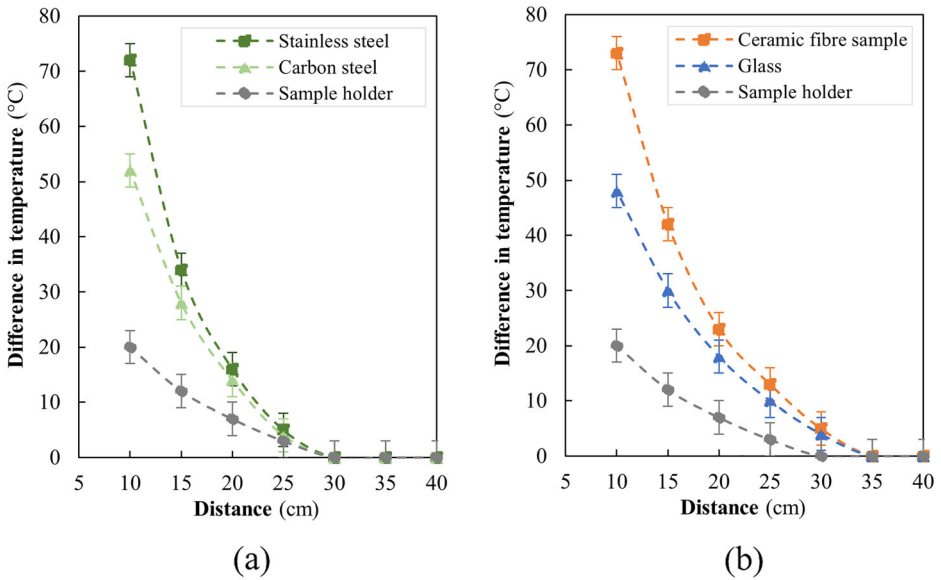
Figure 13. **Difference (increase) of temperature in the heating pads due to the presence of specimens 20 20 cm² together with the specimen holder, as well as the specimen holder itself without a specimen: (a) stainless steel and carbon steel, (b) ceramic fibre and glass.**

distance of 10 cm were recorded, with the case of ceramic fibre and stainless steel being to most critical cases. This is related to the high reflectivity of stainless steel, therefore higher thermal radiation feedback, and the low thermal inertia of the ceramic fibre, therefore the higher surface temperature and radiation feedback.

3.4. Full Power Mode and Thermal Shield

As highlighted in the previous section with regards to the presence of a specimen in front of the heating surface, the same concept applies to the cases in which the heating pads are set in *full power mode* and a thermal shield is placed in front of the heating pads. This provides thermal feedback to the heating pads and affects the temperature evolution of the heating pads since their temperature is not directly controlled. Indeed, as discussed in Sect. 2.2.3, a thermal shield in front of the heating pads influences the net heat gain at the heating pads, mainly affecting the heat losses (primarily radiation in this case).

To investigate the influence of a thermal shield in front of the heating surface, a ceramic fibre blanket (Insulfrax S Blanket—25 mm thick) was placed on the specimen holder, in front of the heating surface, as shown in Fig. 14.

As for the previous configurations, the transient evolutions of the heating pads' temperature and incident heat flux were measured at different distances for *full power mode* in an open environment with the ceramic fibre thermal shield. Fig-
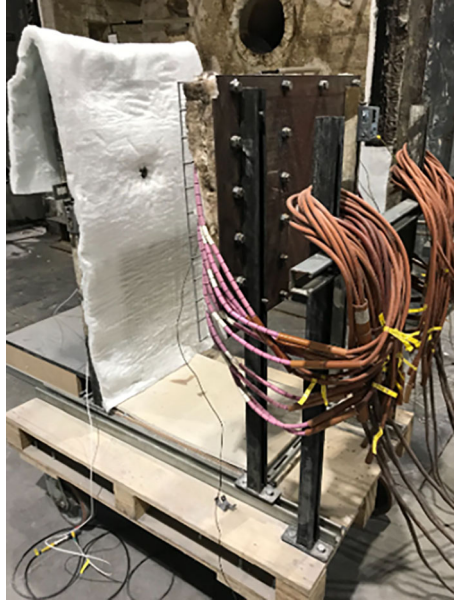
Figure 14.   Photography of the measurement of the incident heat flux with a thermal shield (ceramic fibre) around the heat flux gauge.

ure 15 reports the temperature and heat flux evolutions for the distances 10 cm, 15 cm and 20 cm between the heat flux gauge and the heating pads. In the beginning, the temperature of the heating pads was around 20°C and then the transformer set in the *full power mode* led to a temperature increase in the heating pads and measured incident heat flux. After a stabilisation time for achieving steady-state condition of about 50 min, the heating pads reached higher temperatures than the ones recorded in an open environment (up to 1200°C). Similarly, the heat flux gradually increased, leading to higher values than the ones shown in Fig. 11 for the open environment. Due to the safety and calibration limitations of the heat flux gauge, the measurement was stopped when the heat flux reached 150 kW/m^2.

Consequently, after reaching steady-state temperature in the heating pads after a stabilisation time, the values of incident heat fluxes at different distances for this case with an important thermal shield can be compared to the open environment case, as shown in Fig. 16. The difference between the curves increases with the
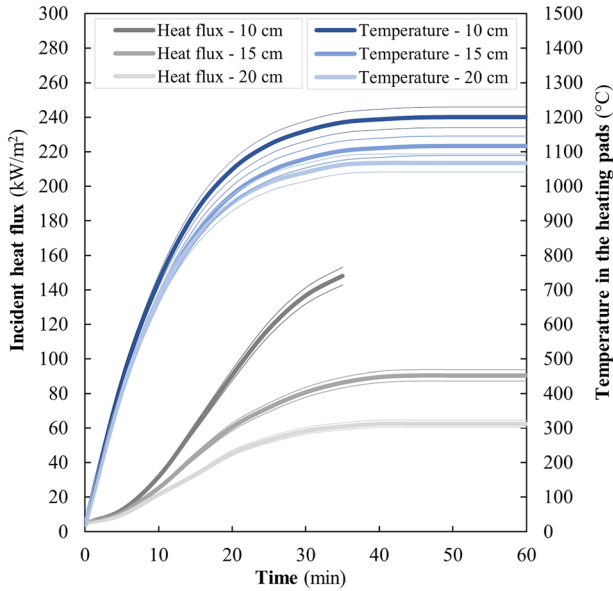
Figure 15. Evolution of the incident heat flux and the temperature in the heating pads for distances 10 cm, 15 cm and 20 cm between the heat flux gauge and the heating pads, with full power mode and with ceramic fibre around the heat flux gauge.
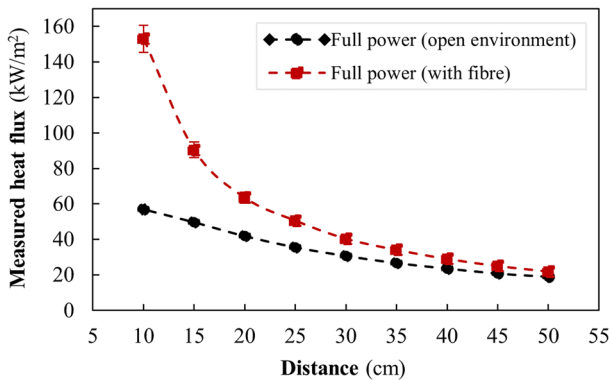

Figure 16. Heat flux measured for various distances between the heating pads and the specimen, for *full power mode*, with an open environment and with ceramic fibre around the heat flux gauge.

decrease in the distance between the heat flux gauge and the heating pads. This is mainly caused by two factors.

The first factor relates to the fact that, during these measurements, the heat flux gauge is fully immersed in the boundary layer of the ceramic fibre. Therefore, the heat flux gauge is measuring not only the radiant heat flux coming from the heat-

ing pads but also a convective component coming from the ceramic fibre. This component is always present in the results shown in Fig. 16 because a difference in the measured heat flux is visible for all distances, despite the fact that, for higher distances, the radiation feedback should become negligible.

The second factor relates to the thermal radiation feedback provided by the ceramic fibre placed in front of the heating surface, which causes a temperature increase in the heating pads as previously noticed at a local level in Sect. 3.3 (refer to Fig. 13). The increase of the temperature of the heating pads was then measured and it is reported in Fig. 17. Even if the material is the same as the one tested in the previous section, the thermal radiation feedback is also dependent on the size of the thermal shield because it affects the view factor. At the same distance, the ceramic fibre placed around the heat flux gauge has a more important influence on the heating pads' temperature than a specimen 20 20 cm^2, as shown in Fig. 17. This effect also becomes more relevant for higher distances: Fig. 17 highlights how the thermal feedback effect is also noticed at a distance of 40 cm, while it is negligible at 35 cm for the 20 20 cm^2 case.

4. Thermal Boundary Conditions

The control and quantification of the thermal boundary conditions at the exposed surface of test specimens have a key role in the assessment and comparison of the performance of construction materials in fire conditions [35]. In addition, the careful characterisation of the thermal boundary conditions is typically a fundamental parameter to be defined in any numerical model for studying the thermo-mechanical behaviour of materials. This section investigates and discusses the thermal boundary conditions imposed by the experimental apparatus in different situations.

4.1. Temperature Control and Open Environment

When the temperature of the heating pads is controlled to a specific level (in this configuration possibly up to 950°C), the heating surface can be considered a radiant source of heat with a quasi-homogeneous temperature and the test specimen is exposed to an incident radiant heat flux at the exposed surface. In the case of an open environment (no other major thermal contributions), the surrounding environment can be considered at ambient conditions and the heating pads' surface the main source of heat. Accordingly, the specimen surface has convective (free natural convection) and radiative heat losses with the surrounding environment and the thermal boundary conditions at the exposed surface of the test specimen can be obtained in a similar manner to many radiant panels applications for fire testing [15, 36]:

$$\dot{q}''_{net} = \alpha \cdot \dot{q}''_{inc} - h_c \left(T_{surf} - T_\infty \right) - F\varepsilon\sigma \left(T_{surf}^4 - T_\infty^4 \right) \tag{1}$$
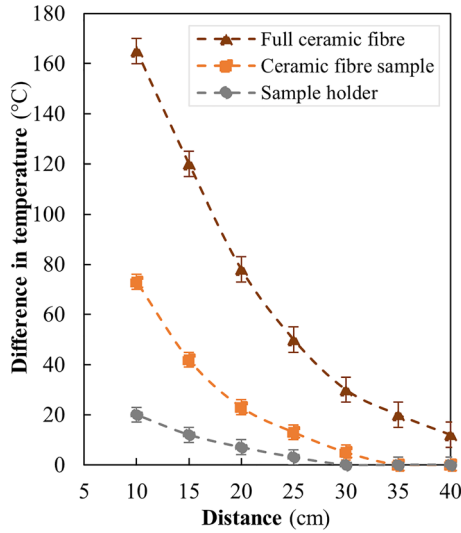
Figure 17. **Difference (increase) of temperature in the heating pads due to the presence of a ceramic fibre specimen (20 20 cm²) together with the specimen holder, full ceramic fibre mat (65 120 cm²) as well as the specimen holder itself without a specimen.**

where $\dot{q}''_{inc}$ [kW/m²] is the incident heat flux at the exposed surface of the test specimen, $\dot{q}''_{net}$ [kW/m²] is net heat flux absorbed by the specimen at the exposed surface, which has a surface temperature equal to T_{surf} [K] and it is surrounded by a gas temperature equal to T_{∞} [K]. The absorptivity and the emissivity of the exposed surface are respectively α [–] and ε [–], and they are usually considered analogous according to Kirchhoff's law [3]. The convective heat losses are described by the convective heat transfer coefficient h_c [W/m²K], which can be estimated using well-established correlations for vertical hot plates [3, 36]. In contrast, the radiative heat losses are considered by the Stefan-Boltzmann constant σ [5.67 10⁻⁸ W/m²K⁴] and the view factor F [–] between the specimen and the far field.

4.1.1. Heat Flux Homogeneity and Specimen Size If the heating surface has a homogenous temperature and the test specimen is smaller than the radiant source of heat, the incident radiant heat flux ($\dot{q}''_{inc}$) can be considered homogeneously distributed over the exposed surface. However, the specimen dimensions have a significant influence on this problem. Indeed, the view factor between the specimen's surface and the heating pads affects the value and distribution of incident heat

flux. In particular, a higher discrepancy is usually achieved between the centre and edges/corners of the test specimens.

Considering the exact size of the heating surface (61 46 cm^2), a theoretical analysis was carried out to calculate the view factor over the exposed surface of test specimens at various distances (from 0 to 50 cm), given different specimen sizes: 10 10 cm^2, 20 20 cm^2 and 30 30 cm^2. Figure 20 presents the results in the form of ratios (in percentage) between the view factors at the centre and the corner of square specimens of various dimensions. The closer to 100% this ratio is, the more uniform the distribution of the incident heat flux over the exposed surface of the specimen.

The results shown in Fig. 18 evidence how using the described heating pads surface, 10 10 cm^2 test specimens have a homogeneous distribution of heat flux, with discrepancies up to 2–3%, and this result is quite independent of the distance between the specimen surface and the heating surface. In contrast, for 30 30 cm^2 specimens, the difference between the view factors, hence the incident heat fluxes, at the centre and at the corners can differ up to 25% and it is highly dependent on the distance, reaching the maximum difference between 20 and 30 cm. Specimens 20 20 cm^2 represent a good compromise for the assembled heating surface, considering the heat flux distribution above 90% and a representative size for bench-scale fire testing. Because of this, this specimen size was chosen for the following experimental campaigns involving this apparatus.

4.1.2. Convective Boundary Layer To verify the defined thermal boundary conditions and the radiation-driven mode of heat transfer, it is important to also examine the convective heat transfer in proximity to the experimental apparatus. In Eq. (1), the convective thermal boundary conditions were set as free (natural) convection with the surrounding environment, assumed at ambient temperature (T_∞). Accordingly, a sufficient spatial separation between the heating pads and the exposed surface of the test specimen must be ensured to enable natural convection and avoid convective heat transfer interaction between the test specimen and the convective boundary layer of the heating pads [15, 36, 37].

This distance should be at least higher than the thickness of the boundary layer of the heating surface and one of the test specimen. The thickness of the specimen's boundary layer depends on the specimen characteristics, primarily the material thermal inertia and the temperature achieved by the specimen surface, as well as a geometrical characteristic length. On the other hand, the boundary layer thickness of the radiant panel composed of heating pads can be estimated following conventional calculations considering it as a vertical hot plate subjected to natural free convection [3]. Assuming the heating pads' surface temperature equal to 900–1000°C, an ambient temperature of 20°C and the panel's vertical characteristic length equal to 46 cm, the thickness of the convective boundary layer of the heating pads panel can be estimated equal to 3.2–3.3 cm. This result was also experimentally confirmed by a qualitative measurement using a linear flag made of several aluminium thin foils and placed orthogonally to the heating surface, as shown in Fig. 19.
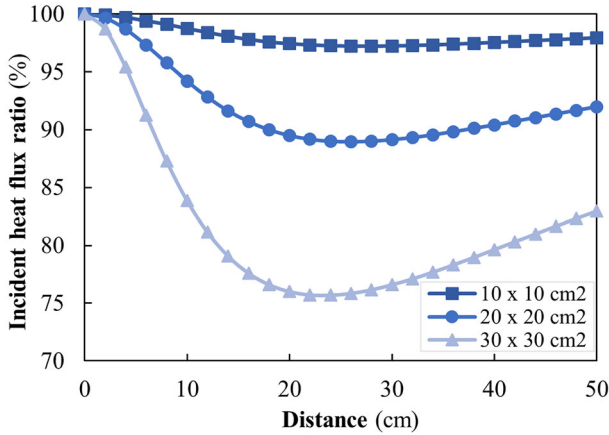
Figure 18. Percentage of the incident heat flux reaching corners of the specimen compared to the incident heat flux reaching the centre of the specimen (100%), depending on the distance between the exposed surface of the specimen and the heating pads.

Figure 19. The zone of convective influence coming from the heating pads—qualitative measurement using a flag made of aluminium thin foil.

This outcome highlights that the convective boundary layer of this experimental apparatus is in the order of magnitude of a few centimetres and free convection can be assumed above these distances (typically 10 cm). These results also underline how the boundary layer of this electrical radiant panel is much thinner than the ones for typical gas-fired radiant panels, typically in the range of 15–20 cm [26, 36, 37].

4.2. Full Power Mode and Thermal Shield

If the transformer is set in *full power mode*, the temperature on the heating pads is not automatically regulated and it might change depending on various factors (as explained in Sect. 2.2.3). Similarly, the presence of test specimens and the use of a thermal shield (e.g. ceramic fibre around the specimen) can highly influence the thermal conditions of the heating pads and the tested specimen. As a result, the thermal boundary conditions presented in Sect. 4.1 cannot be applied and their definition becomes much more complex.

Indeed, all the modes of heat transfer defined in Eq. (1) may be affected by the temperature of the heating pads, hence influence the incident radiant heat flux, the specimen surface temperature, the thickness of the convective boundary layer as well as the convective heat transfer coefficient, and the radiation losses. In addition, when a thermal shield (e.g. ceramic fibre) is placed around the specimen (Sect. 3.4), there is an important effect of convection flows caused by the surrounding material, as well as additional feedback from the shield to the heating pads.

All these effects have to be taken into account for the definition of the thermal boundary conditions. This exercise becomes quite challenging due to the complexities in measuring specific values (e.g. temperature of the heating pads and incident heat flux at specimen surface) and defining physical parameters (e.g. convective heat transfer coefficient). This problem can be solved in an implicit manner starting from experimental results.

5. Bench-Scale Fire Tests

After the description and the characterisation of the heating conditions reproduced by the developed experimental apparatus, a few bench-scale specimens of various construction materials are tested in order to investigate the capabilities of the presented methodology and the imposed thermal boundary conditions. In addition, the experimental results are compared to numerical models to study the heat transfer problem and the accuracy of the definition of the thermal boundary conditions.

The example presented herein discusses the experimental application of the well-defined thermal boundary conditions, hence incident radiant heat flux, in accordance with Sect. 4.1.

5.1. Experimental Setup and Test Method

This case study aims at reproducing the thermal boundary conditions defined in Eq. (1) and therefore avoiding the influence of the thermal feedback of the test specimen and the influence of any other thermal shield (e.g. ceramic fibre). According to the results discussed in Sect. 3, the distance between the heating pads and the exposed surface was set to 25 cm, and the heating pads were heated using the automatic mode with a heating rate of 1000°C/h and a target temperature of 925°C. Test specimens were kept in place using the described specimen

holder and without any insulation around the specimen ("open environment"). According to the calibration presented in Sect. 3.1, this configuration aimed at imposing an incident radiant heat flux of 30 kW/m² at the exposed surface of test specimens.

The specimens tested in this research study were 20 20 cm² carbon steel plates (thickness 5 mm), 20 20 cm² stainless steel plates (thickness 2 mm), as well as 20 20 cm² glass plates (thickness 6 mm), as shown in Fig. 20. Two thermocouples (type K, diameter 0.5 mm) were welded in the centre of the exposed surfaces of stainless steel and carbon steel specimens to measure the increase in temperature during the test. In contrast, the same thermocouples were glued on the exposed surface of the glass specimens using FixWool FX adhesive, a glue designed for high temperature applications (up to 1300°C) and characterised by high homogeneity and easiness of application.

The tests were performed in two configurations for the thermal boundary conditions at the unexposed surface (back). First, specimens of each material were tested with the unexposed surface free (fully exposed to ambient conditions). Second, specimens of each material were tested with a layer of 20 20 cm² ceramic fibre (Insulfrax S Blanket—25 mm thick), placed and ensured in contact with the unexposed surface of the specimen.

The testing procedure foresees that, at the beginning of each test, a protecting plate was placed between the heating pads and the specimen, at about 40 cm distance from the heating pads in order to limit its influence on the temperature of the heating pads and to protect the test specimen (shown in Fig. 21a). The protecting plate was then removed when the temperature of the heating pads reached the target temperature of 925°C and steady-state conditions were established (stabilisation time of 55 min) and the distance between the specimen and the heating pads was adjusted to the desired 25 cm (shown in Fig. 21b). The thermal tests were performed for 30 min after the removal of the protecting plate.

5.2. Numerical Modelling

In order to verify the accuracy of the thermal problem defined in the experiments, a numerical model was established based on Eq. (1), considering a unit view factor (F) and neglecting the radiative heat gains from the far field [15]. The software used to establish the numerical model was Abaqus 2019 [38]. Accordingly, the net heat flux absorbed by the specimen at the exposed surface ($\dot{q}''_{net}$) can be calculated as:

$$\dot{q}''_{net} = \alpha \cdot \dot{q}''_{inc} - h_c \left(T_{surf} - T_\infty \right) - \varepsilon \sigma T^4_{surf} \tag{2}$$

As illustrated in Fig. 22, two cases for each tested material were modelled as one-dimensional heat transfer with varying thermal boundary conditions at the unexposed surface of test specimens. The first case referred to the tests with a free unexposed surface of the specimen, where convective ($\dot{q}''_{loss,conv}$) and radiative ($\dot{q}''_{loss,rad}$) losses were considered (see Fig. 22a). For the case with ceramic fibre insulation, the conductive losses ($\dot{q}''_{back}$) were calculated at the unexposed surface
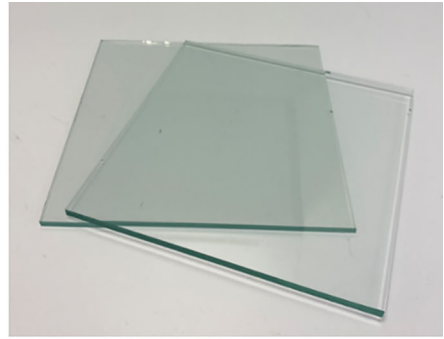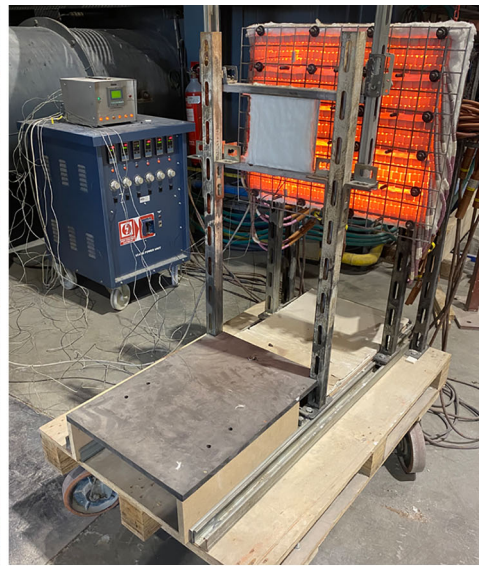
Figure 20. Photography of specimens tested: (a) carbon steel and stainless steel plates with welded thermocouples, (b) glass plates.

Figure 21. Photography of a bench-scale test: (a) during the heating process of the panel, with an insulation plate between the specimen and the heating pads, (b) during the specimen exposure.

of the specimen considering the thermal properties of the insulation material and including again convective and radiative losses at the back surface (see Fig. 22b).

In order to solve the heat transfer problem, various input parameters were defined. As regards the thermo-physical properties, the materials properties of
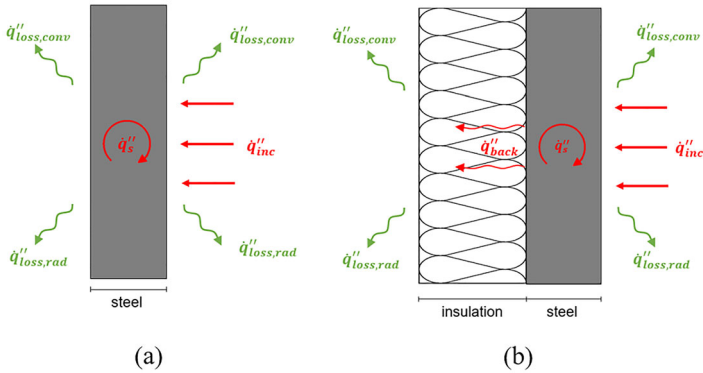
Figure 22. Schematic drawings of boundary conditions modelled: (a) free unexposed surface, (b) fibre placed on the unexposed surface; $\dot{q}''_s$ refers to heat storage within the specimen and $\dot{q}''_{back}$ refers to conductive heat transfer from the specimen to the fibre.

ceramic fibre were defined as constant for density and specific heat capacity, and function of temperature for thermal conductivity, as shown in Table 2. The properties of carbon steel and stainless steel [28] as well as the properties of glass [29, 33] were included as functions of temperature.

The emissivity and absorptivity of carbon steel were set as 0.7 [28], 0.4 for stainless steel [28], and 0.6 for ceramic fibre [32]. The glass absorptivity was defined according to Table 1 in the case of a free unexposed surface, while the emissivity value (absorptivity + transmissivity) was used for the case with the insulated unexposed surface since glass could not transmit heat wave due to the opaque substrate. Finally, the convective heat transfer coefficient was set equal to 10 W/m² K, both for the exposed and unexposed surfaces, using empirical correlations found in the literature [3].

5.3. Experimental and Numerical Results

The numerical results and the temperature evolutions measured in the bench-scale tests are presented in Fig. 23a for carbon steel, Fig. 23b for stainless steel and Fig. 23c for glass specimens. The temperature evolutions obtained experimentally are shown as temperature ranges which include the measurement inaccuracies based on readings of thermocouples attached to the same specimen ($\pm$ 5°C) and the thermocouple accuracy specified by the producer ($\pm$ 4°C up to 1000°C). On the other hand, the temperature evolutions obtained numerically include the inaccuracy of the heat flux definition, shown in Fig. 10 ($\pm$ 1.5 kW/m² for the test conditions described in Sect. 5.1) which are presented as shaded areas. It is also important to mention other uncertainties not included in the plot. For instance,

Table 2
Thermal Properties of Ceramic Fibre

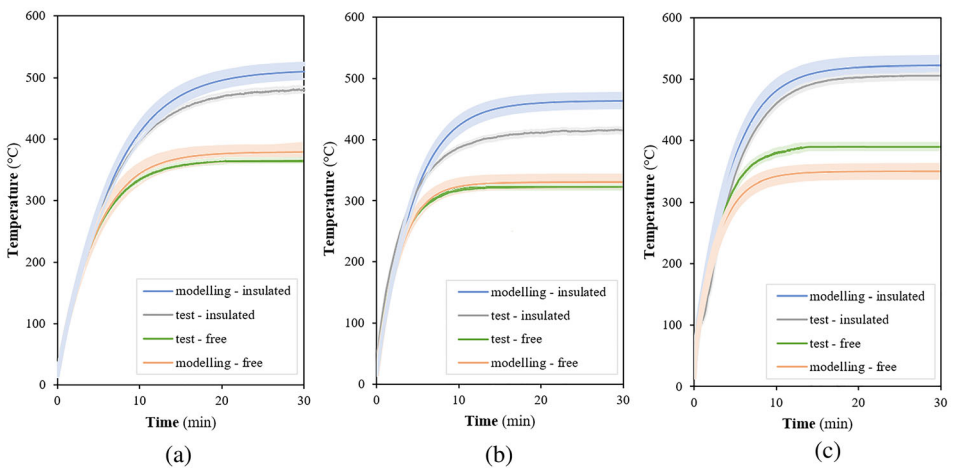|	
Density (kg/m^3)	128 [30]
Specific heat (J/kg K)	1000 [31]
Thermal conductivity (W/m K)	[30]
20℃	–
200℃	0.05
400℃	0.08
600℃	0.12
800℃	0.18
1000℃	0.29

Figure 23. **Temperature evolution on the exposed surface of the specimen, compared to the temperature evolution obtained through numerical modelling: (a) carbon steel, (b) stainless steel, (c) glass.**

the value of the convective heat transfer coefficient is kept as an approximated constant value (10 W/m^2 K on both sides) while in reality, it may vary during the test and from test to test and is dependent on many factors: conditions in the laboratory (e.g. flow fields), and specimen geometry (e.g. size and orientation). Moreover, the thermo-physical properties of tested materials, especially the properties of the ceramic fibre used to insulate the unexposed surface, are applied as either constants or values for certain temperature points. These properties are highly temperature- and product-dependent, and they largely vary depending on the referenced source. Additionally, some attention has to be paid to the glass transmission coefficient which may vary depending on the glass composition, surface

treatment and emissivity spectrum of the heat source. For the current simulations, this coefficient was taken from the literature.

As regards the carbon steel and stainless steel plates with free unexposed surfaces, the experimental results for both types of steel are very comparable with the numerical results (± 15°C), confirming the correct definition and estimation of the thermal boundary conditions at the test specimens and imposed by the developed experimental apparatus.

In contrast, the specimens tested with fibre on the unexposed surface achieved significantly lower temperatures after 30 min than what was obtained in the numerical simulations (about ± 50°C compared to temperatures of specimens modelled with fibre). The reason for this difference could be related to the underestimation of the conductive heat losses at the substrate insulation in the numerical model (steady-state thermal conductivity values were used) and the insufficient contact between the test specimen and the ceramic fibre, which could have resulted in heat losses at the connecting interlayer.

On the other hand, both configurations with glass specimens obtained similar temperature evolutions as in numerical modelling (± 40°C for free specimen and ± 16°C for insulated specimen). The differences might be caused by the presence of non-transparent glue used for the thermocouple attachment and inaccuracies in the definition of the glass optical surface properties (e.g. absorptivity, transmissivity, and emissivity), which highly depend on many factors (e.g. radiation emissivity spectrum).

6. Discussion

The previous sections have presented and discussed the experimental apparatus for bench-scale fire testing that uses electrical heating pads. From the various analyses and experimental results, it is possible to highlight different advantages and shortcomings of the presented apparatus compared to other bench-scale methodologies that involve radiant panels and primarily radiative heat fluxes for fire testing.

6.1. Advantages

In addition to the relatively low cost, this research study has first underlined the ease of using radiant panels for fire testing bench-scale specimens, along with their flexibility and modularity for many research applications.

The safe environmental conditions that can be easily achieved using this apparatus were also stressed. No combustion and hazardous gases are released by the electricity-powered heating pads, whereas these are usually produced by gas-fired radiant panels. This could represent a hazardous situation in the case of laboratories without a dedicated extraction system and/or with limited dimensions. Moreover, this solution avoids any complications related to the installation and storage of flammable gases.

Also, it was shown how the supplied electrical power and the heating pads' temperature, therefore the thermal boundary conditions, can be controlled in a

precise manner up to the heating pads' temperature of 950℃, owing to the automatic regulation system of the transformer.

Furthermore, experimental results have emphasised how the thickness of the convective boundary layer of the heating surface is significantly lower than with gas-fired radiant panels. This significantly reduces the area of convective influence and enables to test specimens at lower distances between the exposed specimen surface and the heating pads and achieve higher heat fluxes, still avoiding the interaction between the boundary layers of the specimen and the heating pads, and directly control the thermal boundary conditions imposed on specimens.

The described apparatus is highly-modular and mobile, and it can be used in most circumstances and laboratories, assuming sufficient available electrical power and electrical safety precautions. When fire testing non-combustible materials, the apparatus does not require an exhaust system to collect combustion gases and smoke, a requirement that limits the application and flexibility of using gas-fired radiant panels.

6.2. Limitations

The apparatus certainly requires the availability of important electrical power. However, the electrical power required for this apparatus falls within the typical capabilities of major laboratories and the power required to feed the 0.28 m^2 heating surface is well below the 65 kVA capacity of the transformer.

Due to the high thermal inertia of the heating pads, the heating and cooling processes are quite time-consuming. The heating pads take about 15 min to achieve a homogeneous steady-state temperature of 800℃ over its surface and this process can take more than 45 min for higher temperatures or for *full power mode*. In addition, the apparatus typically takes 1.5–2 h to decrease its temperature back to ambient conditions between successive tests, unless forced convection is applied for cooling (e.g., mechanical fan or compressed air).

While the maintenance of the apparatus is quite limited and low in cost, the heating pads and the steel grid may require frequent replacement in case of intense and prolonged use.

One of the main limitations of this apparatus is the fact that the temperature of the heating pads, and therefore the thermal boundary conditions, can be controlled only up to 950℃. This results in a relatively low range of incident heat fluxes for fire testing, with values up to approximately 50 kW/m^2. However, if higher heat fluxes and temperatures have to be achieved, it is possible to set the heating pads in *full power mode*. In this case, the temperature of the heating pads, and therefore the incident heat flux, are not directly controlled and the testing conditions are affected by many factors: for instance, the presence of a specimen, the type of the specimen, the size of the specimen, the presence of thermal shields, and the distance between the specimens and heating pads. This increases the experimental uncertainties and causes a lower understanding and control of the thermal boundary conditions, but it extends the capabilities and application of the experimental apparatus.

6.3. *Future Possibilities*

The high flexibility and modularity of the presented apparatus can enable many other future applications for investigating the behaviour of various construction materials and systems exposed to fire and/or elevated temperatures.

Among many possibilities, the heating surface and test specimens can be increased in size. It is easy to increase the heating surface dimension by adding and connecting more heating pads. Using the described transformer, it would be possible to create a heating surface of 0.67 m^2 (two layers) or even a heating surface of 1.34 m^2 (one layer). This would enable testing specimens of higher dimensions and obtaining higher heat fluxes at the same distance.

The heating pads can be also configured to work using different heating zones over the radiant surface. The transformer allows to create up to six different temperature zones on the heating pads, creating different temperature gradients and various distributions of heat fluxes over the exposed surface of test specimens. For example, this application can be useful to recreate specific glass breakage patterns caused by temperature gradients.

Finally, the heating surface can be installed in an enclosure with controlled environmental conditions. This would allow for testing materials and systems in different environmental conditions, for example in controlled oxygen or nitrogen atmosphere, low-pressure chamber and/or various humidity levels. This is the case for the cone calorimeter, of which a customised version has already been designed for this purpose, showing a possible direction for future development of this experimental apparatus [40].

7. Conclusions

This research study presents an experimental methodology that uses electrical heating pads for fire testing bench-scale samples, characterised by lower costs compared to well-known gas-fired radiant panels apparatus (e.g. H-TRIS), but still enabling high experimental repeatability and versatility for many applications. The research study analyses its functionalities, including the testing methodology and the characterisation of the heating conditions. The presented experimental apparatus imposes specific thermal boundary conditions by controlling the temperature of the heating pads and a large range of heating conditions can be imposed on test specimens for investigating the behaviour of modern construction materials and systems exposed to fire and/or elevated temperatures.

Three modes of testing were described: controlled temperature in an open environment, full power mode in an open environment (with or without a specimen) and full power mode with a thermal shield. On one hand, the first mode is very useful for any type of systematic research due to the well-defined thermal boundary conditions, ensuring a comprehensive and robust approach. On the other hand, the other two modes are more suitable for internal R&D projects which aim at imposing higher heat flux and achieving higher temperatures, at the cost of compromising the well-defined boundary conditions. These projects usually focus on pushing the limits of materials and systems in order to understand changes in

fire behaviour and how to improve them. In the end, the choice of a suitable mode depends on the needed approach and aim of the tests.

There are many important advantages of the described apparatus: among others, its relatively low cost and its flexibility and modularity for many research applications. There are various disadvantages as well, i.e. thermal inertia of the heating pads. The apparatus characteristics, along with its main advantages and limitations described in this study, provide an extensive overview of its capabilities and potential applications. It is crucial to consider all features of the apparatus when choosing as testing equipment and method for a specific research program.

Acknowledgements

Declarations

Conflict of interest   The authors declare no conflicts of interest.

Open Access

References

1. Drysdale D (2011) An introduction to fire dynamics. Wiley, 2nd edn. https://doi.org/10.1002/9781119975465
2. Comité Européen de Normalisation (2020) EN 1363–1:2020—fire resistance tests—part 1: general requirements. Belgium, Brussels
3. Incropera FP, DeWitt DP, Bergman TL, Lavine AS (2006) Fundamental of heat and mass transfer. Wiley, 6th edn

4. International Organization for Standardization (2019) ISO 5660–2:3025 reaction-to-fire tests—heat release, smoke production and mass loss rate. vol. 3, no. January, p 64
5. Hurley M, et al (2016) SPFE handbook of fire protection engineering. Springer, 5th edn
6. International Organization for Standardization (2011) ISO 12136:2011—reaction to fire tests—measurement of material properties using a fire propagation apparatus
7. American Society for Testing and Materials (2019) ASTM E2058–19—standard test methods for measurement of material flammability using a fire propagation apparatus (FPA). West Conshohocken, Pennsylvania
8. International Organization for Standardization (2010) ISO 9239–1:2010—reaction to fire tests for floorings—part 1: determination of the burning behaviour using a radiant heat source
9. American Society for Testing and Materials (2020) ASTM E648–19ae1—standard test method for critical radiant flux of floor-covering systems using a radiant heat energy source. West Conshohocken, Pennsylvania
10. International Organization for Standardization (2006) ISO 5658–2:2006—reaction to fire tests—spread of flame—part 2: lateral spread on building and transport products in vertical configuration
11. American Society for Testing and Materials (2019) ASTM E1317–19—standard test method for flammability of surface finishes. West Conshohocken, Pennsylvania
12. American Society for Testing and Materials (2018) ASTM E1321–18—standard test method for determining material ignition and flame spread properties. West Conshohocken, Pennsylvania
13. Sakji S (2006) Modélisation probabiliste et validation expérimentale du transfert thermique et du comportement thermomécanique d'une plaque multicouche carton-plâtre-carton soumise au feu. Dissertation, University of Marne-La-Vallée, France
14. Sakji S, Soize C, Heck JV (2008) Probabilistic uncertainty modeling for thermomechanical analysis of plasterboard submitted to fire load. J Struct Eng 134(10):1611–1618. 10.1061/(ASCE)0733-9445(2008)134:10(1611)
15. Maluk C, Bisby L, Krajcovic M, Torero JL (2019) A heat-transfer rate inducing system (H-TRIS) test method. Fire Saf J 105:307–319. 10.1016/j.firesaf.2016.05.001
16. Rickard I, Spearpoint M, Lay S (2020) The performance of laminated glass subjected to constant heat fluxes related to building fires. Fire Mater 45(2):283–295. 10.1002/fam.2939
17. Mohammed H, Ahmed H, Kurda R, Alyousef R, Deifalla AF (2022) Heat-induced spalling of concrete: a review of the influencing factors and their importance to the phenomenon. Materials 15(5):1693. 10.3390/ma15051693
18. Maluk C, Bisby L, Terrasi GP (2017) Effects of polypropylene fibre type and dose on the propensity for heat-induced concrete spalling. Eng Struct 141:584–595. 10.1016/j.engstruct.2017.03.058
19. Mohammed H, Sultangaliyeva F, Wyrzykowski M, Terrasi GP, Bisby L (2023) Heat-induced explosive spalling of self-prestressing, self-compacting concrete slabs. Constr Build Mater 372:130821. 10.1016/j.conbuildmat.2023.130821
20. Lucherini A, Maluk C (2019) Assessing the onset of swelling for thin intumescent coatings under a range of heating conditions. Fire Saf J 106:1–12. 10.1016/j.firesaf.2019.03.014
21. Lucherini A, Lam HY, Jimenez M, Samyn F, Bourbigot S, Maluk C (2022) Fire testing of intumescent coatings: comparison between bench-scale furnace and radiant panels experimental methodologies. Fire Technol 58:1737–1766. 10.1007/s10694-022-01216-3
22. Hidalgo JP, Welch S, Torero JL (2015) Performance criteria for the fire safe use of thermal insulation in buildings. Constr Build Mater 100:285–297. 10.1016/j.conbuildmat.2015.10.014

23. Lucherini A, Hidalgo JP, Torero JL, Maluk C (2021) Influence of heating conditions and initial thickness on the effectiveness of thin intumescent coatings. Fire Saf J 120:103078. 10.1016/j.firesaf.2020.103078
24. Lucherini A, Razzaque QS, Maluk C (2019) Exploring the fire behaviour of thin intumescent coatings used on timber. Fire Saf J 109:102887. 10.1016/j.firesaf.2019.102887
25. Lucherini A, Torero JL, Maluk C (2020) Effects of substrate thermal conditions on the swelling of thin intumescent coatings. Fire Mater . 10.1002/fam.28
26. Mohammed H, Morisset D, Law A, Bisby L, (2021) Quantification of the thermal environment surrounding radiant panel arrays used in fire experiments. Proceedings of the 12th Asia-oceania symposium on fire science and technology (AOSFST), Brisbane, Australia
27. Lucas J (1999) Infrared glasses. Curr Opin Solid State Mater Sci 4(2):181–187. 10.1016/s1359-0286(99)00007-8
28. Comité Européen de Normalisation (2005) EN 1993-1-2: Eurocode 3: design of steel structures—part 1–2: general rules—structural fire design. Belgium, Brussels
29. AGC technical data sheet—Planibel glass (2011). https://www.savas.it/uploads/products/agc-planibel-scheda-tecnica.pdf. Accessed April 2023
30. Keramab Insulfrax S Blanket—technical data sheet
31. Unifrax Insulfrax S Blanket—Product information sheet, https://www.unifrax.com/wp-content/uploads/2018/08/C-1462.pdf. Accessed April 2023
32. Benko I (1999) Energy conservation through increased emissivity in furnaces. Period Polytech Mech Eng 35(4):235–245
33. Debuyser M, Sjöström J, Lange D, Honfi D, Sonck D, Belis J (2017) Behaviour of monolithic and laminated glass exposed to radiant heating. Constr Build Mater 130:212–229. 10.1016/j.conbuildmat.2016.09.139
34. Honfi D, Sjostrom J, Bedon Ch, Kozøowski M (2022) Experimental and numerical analysis of thermo-mechanical behaviour of glass panes exposed to radiant heating. Fire 5:124. 10.3390/fire5040124
35. Torero JL, Law A, Maluk C (2017) Defining the thermal boundary condition for protective structures in fire. Eng Struct 149:104–112. 10.1016/j.engstruct.2016.11.015
36. Lucherini A (2020) Fundamentals of thin intumescent coatings for the design of fire-safe structures. Dissertation, School of Civil Engineering, The University of Queensland. https://doi.org/10.14264/uql.2020.1021
37. Laschütza T (2017) Numerical and experimental investigation of a thin skin calorimeter (TSC). MSc Thesis, School of Engineering, University of Edinburgh
38. Dassault Systèmes Simulia Corp (2019) Abaqus/CAE
39. Comité Européen de Normalisation (2002) EN 1991-1-2: Eurocode 1: actions on structures—part 1–2: general actions—actions on structures exposed to fire. Belgium, Brussels
40. Babrauskas V, Twilley W, Janssens M, Yusa S (1992) A cone calorimeter for controlled-atmosphere studies. Fire Mater 16:37–43. 10.1002/fam.810160106